Hindawi
Geofluids
Volume 2022, Article ID 3679384, 17 pages
https://doi.org/10.1155/2022/3679384

Research Article

Numerical Assessment on Unloading Disturbance and Gas Extraction in Remote Distance Protective Layer Mining

Zhigang Yuan,[1,2,3] **Zehua Jiang**,[1] **Shuqing Li**,[1,2,3] **Jintao Zhao**,[1] **and Fei Huang**[1,2,3]

[1]*School of Resources, Environment and Safety Engineering, Hunan University of Science and Technology, Xiangtan 411201, China*
[2]*Work Safety Key Lab on Prevention and Control of Gas and Roof Disasters for Southern Coal Mines, Hunan University of Science and Technology, Xiangtan 411201, China*
[3]*Hunan Provincial Key Laboratory of Safe Mining Techniques of Coal Mines, Hunan University of Science and Technology, Xiangtan 411201, China*

Correspondence should be addressed to Zhigang Yuan; cquyzg@163.com

Received 6 May 2022; Accepted 8 July 2022; Published 16 August 2022

Academic Editor: Yingfeng Sun

Protective layer mining could not only significantly alter geostress but also increase the permeability of protected layer, which is beneficial for the coal gas extraction rate and ensures coal mining safety. However, due to unique geologic conditions, remote distance protective layer mining has its own characteristics. To investigate characteristic changes caused by remote distance protective layer mining, a suitable mathematical model that considered disturbance of unloading mining and solid-gas coupling effects during gas extraction was developed. The established mathematical model was implemented by combining FLAC^{3D} and COMSOL programs to study characteristic changes during remote distance protective layer mining of Chajiaotan coal mine. Numerical simulation results of unloading disturbance mining indicated that the protected layer would experience a process of stress loading, stress unloading, stress recovery, and stress stability as the working face of protective layer advanced; unloading disturbance has a greater influence on coal permeability than gas pressure; gas extraction measure should be further adopted to decrease gas pressure. Numerical comparisons of gas pressure distribution in the original protected layer and unloading protected layer revealed that gas extraction after unloading disturbance can reduce gas pressure more effectively, and appropriate borehole spacings in the fully pressure-relief and nonfully pressure-relief zones are 30 m and 5 m, respectively. The layout of field boreholes for gas extraction was designed according to numerical results. The results of site investigation showed that numerical simulation results of relative expansion deformation and gas extraction radii agree well with the results of site observation, demonstrating reliability of the mathematical model and its implementation. The proposed mathematical model is promising for assessing unloading disturbance and gas extraction in remote distance protective layer mining.

1. Introduction

Coal is of significance for the development of China's society and economy [1]. However, with coal mining intensity increasing, hazard of coal and gas outburst would also be increased, which severely influences the efficiency and safety of coal mine production. Hence, disaster control of gas outburst is urgent for coal mining. As is well-known, gas extraction measures have been extensively employed to reduce gas content, and the extraction rate is primarily determined by the coal permeability [2, 3]. Nevertheless, permeability of coal seams in China is relatively lower, which means they are not suitable for gas extraction in their natural state [4]. At present, many artificial permeability enhancement measures have been adopted to improve the coal permeability, such as hydraulic flushing, hydraulic fracturing, and liquid CO_2 phase change fracturing [5, 6]. However, these measures have specific application conditions and shortcomings [7]. When there are several minable coal seams existing in a coal mine, protective layer mining has been regarded as an effective and economic measure to eliminate outburst risk [8], as it leads to geostress relief of protected layer and then significantly enhances the permeability of protected layer, providing a favorable gas extraction condition for protected

layer [9, 10]. Recently, many advances have been achieved on protection effect of protected layer based on numerical modelling, theoretical study, and site investigation. Wang and Zhou [11] proposed a mining stress disturbance factor and obtained the evolution law of mining-induced stress in deep coal bodies during protective layer mining based on numerical simulation. Cai et al. [12] investigated stress distribution law of close distance protected layer using the FLAC^{3D} software and stated that lower protected layer would experience a process of stress loading, stress unloading, and stress recovery with stresses presenting an "O" shape distribution. Pang et al. [13] used a stress disturbance coefficient to characterize mining disturbance intensity and determined disturbance intensity zoning and mining stress evolution law employing discrete element method. Xue et al. [14] established a relationship between volumetric strain and coal permeability and studied permeability evolution law of protected layer as working face of protective layer advanced, revealing that distribution characteristics of coal volume strain and permeability in protected layer were similar. Xie et al. [15] raised a permeability enhancement rate, based on which distributions of permeability enhancement rate of overlying strata during mining were quantitatively analyzed. Yang et al. [16] investigated deformation and fracture characteristics of overlying close distance strata based on a proposed permeability function with damage considered, and laws of coal permeability and gas flow of target strata were obtained. Using the regression analysis method and considering the fracture constitutive relationship, Zhang et al. [17] proposed a permeability function in form of stress. Liu et al. [18] studied the gas extraction processes in coal seams under original and unloading states using COMSOL and indicated that gas extraction in coal seam with remote unloading disturbance has a better effect than that of original coal seam without disturbance. Liu et al. [19] put forward an index called equivalent relative interval to subdivide protective layer mining into three types, and engineering practices of protective layer mining in China were systematically summarized. In conclusion, existing literature primarily focused on close distance protective layer mining, in which either stress evolution laws or gas extraction processes were studied independently; moreover, the permeability evolution models for coal seam adopted in numerical simulation were mostly derived from the coalbed methane exploitation field. However, for protective layer mining, the effect of unloading disturbance and gas extraction should be considered as a unified process, because the stress and pressure states of the protected layer after unloading disturbance would differ significantly from the original state; i.e., initial conditions for gas extraction should be taken from the obtained results resulting from unloading disturbance. Nonetheless, to the best of our knowledge, a unified study in combination with characteristic changes caused by unloading disturbance of protective mining and gas extraction has received little attention. Furthermore, as the gas migration environment would differ in coal mines with varying interlayer distances, remote distance protective layer mining has its own characteristics due to specific geologic conditions [8]. In short, the unloading disturbance and gas extraction in remote distance protective layer mining are not fully understood, so an in-depth investigation is required. In the remainder of this paper, the engineering background is introduced in Section 2; a suitable mathematical model that considers unloading disturbance of remote distance protective layer mining and solid-gas coupling effects during gas extraction is developed in Section 3; the characteristic changes during remote distance protective layer mining and gas extraction are investigated in Section 4; field application and validation are carried out in Section 5; relevant conclusions are drawn in Section 6.

2. Engineering Background

This research is focused on the engineering background of Chajiaotan coal mine, which is located at Guxu mining area of Luzhou City, Sichuan province. Two coal seams called C_{19} and C_{25} coal seams are minable. The C_{19} coal seam is overlying the C_{25} coal seam with interlayer distance being 26.6 m. The average thickness of C_{19} and C_{25} coal seams is 2.0 m and 1.0 m, respectively, with average dip angle being 20°. The original gas pressures of C_{25} and C_{19} coal seams are 0.95 MPa and 2.06 MPa, respectively. The geographical position and lithology columnar of Chajiaotan coal mine are illustrated in Figure 1. According to the literature [20], C_{25} coal seam (referred to as protective layer) with lower outburst risk is first mined, as it would improve the permeability and reduce gas pressure of C_{19} coal seam (referred to as protected layer) in combination with subsequent gas extraction, leading to decrease of gas outburst risks in C_{19} coal seam.

According to relevant studies [8], the unloading effect induced by protective layer mining varies with interlayer distance, resulting in different gas migration environments in the protected layer. Lower protective layer mining is subdivided into three types, as shown in Table 1 [19].

The equivalent relative interval R is calculated by [19]:

$$R = \frac{S}{M}\frac{1}{K\beta_1\beta_2\beta_\alpha}, \tag{1}$$

where S represents the interlayer distance, m; M represents the protective layer thickness, m; K represents the coefficient of roof management; β_1 represents the influence coefficient of mining height; β_2 is the content coefficient of hard rock between the protected layer and protective layer; and β_α represents the coefficient of dip angle; i.e., when dip angle of protective layer $\alpha < 60°$, $\beta_\alpha = \cos\alpha$; otherwise, $\beta_\alpha = \sin(\alpha/2)$.

Based on protective layer mining condition of Chajiaotan coal mine, where $S = 26.6$ m, $M = 1.0$ m, $K = 1$ m, $\beta_1 = 1$, $\beta_2 = 1$, and $\beta_\alpha = 0.94$, then the calculated equivalent relative interval R is 28.3. It indicates that the classification type of Chajiaotan coal mine is a remote distance protective layer, which also implies that C_{19} coal seam is near edge of fractured zone and bending zone.

3. Description of Mathematical Model

3.1. Mathematical Model for Unloading Disturbance of Remote Distance Protective Mining. Coal permeability is a

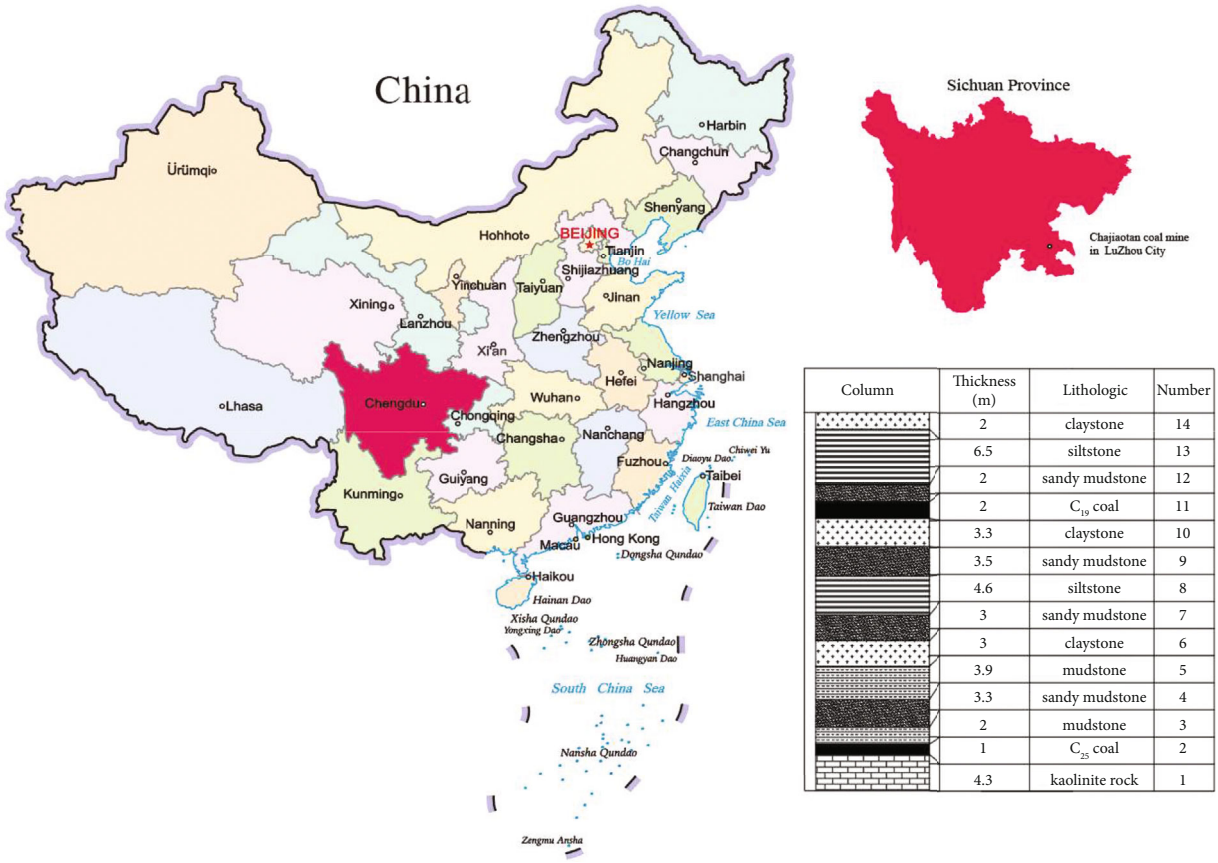

Column	Thickness (m)	Lithologic	Number
	2	claystone	14
	6.5	siltstone	13
	2	sandy mudstone	12
	2	C_{19} coal	11
	3.3	claystone	10
	3.5	sandy mudstone	9
	4.6	siltstone	8
	3	sandy mudstone	7
	3	claystone	6
	3.9	mudstone	5
	3.3	sandy mudstone	4
	2	mudstone	3
	1	C_{25} coal	2
	4.3	kaolinite rock	1

Figure 1: Geographical position and lithology columnar of Chajiaotan mine.

Table 1: Classification method.

Classification type	Equivalent relative interval	Location of protected layer
Super-remote protective layer	$40 < R \le R_{max}$	Bending zone
Remote distance protective layer	$20 < R \le 40$	Edge of bending zone and fractured zone
Close distance protective layer	$R_{min} < R \le 20$	Lower and middle location of fractured zone

significant factor that affects gas extraction effect [4, 5]. In general, a measure of gas extraction should be used prior to decrease the gas content before coal mining. Nonetheless, only a small percentage of adsorption gas could desorb because gas pressure changes little during gas extraction of low permeability coal seams before unloading. Lower protective mining, on the other hand, would effectively cause stress variation of overlying strata, resulting in strata expansion, development, and coalescence of mining-induced fissures. Figure 2 depicts a typical diagram of lower protective layer mining, based on which characteristic changes during unloading disturbance of protective layer mining are explained.

3.1.1. Evolution Model for Permeability. According to ground control theory [19, 21], the surrounding rock of protective layer after coal mining can be subdivided into three different zones, as shown in Figure 2. When protected layer is near or above the boundary of bending zone and fractured zone, as in the case of C_{19} protected layer, whose roof and floor are still relatively complete, original gas can be assumed to be still stored in protected layer. During remote distance protective layer mining, permeability evolution of protected layer involves two stages. The first stage is the unloading disturbance caused by protective layer mining, and the second stage is the effects of gas-solid coupling during gas extraction after unloading disturbance. The influence of gas-solid coupling on permeability at the first stage is minor and ignored. The permeability evolution of protected layer because of unloading disturbance is given by [22]:

$$k = \begin{cases} k_0^{b_\sigma(\Delta\Theta)}, \Theta > \Theta_0, \\ \left(1 + \dfrac{\Theta_0 - \Theta}{\Theta}\xi\right) k_0, \Theta \le \Theta_0, \end{cases} \quad (2)$$

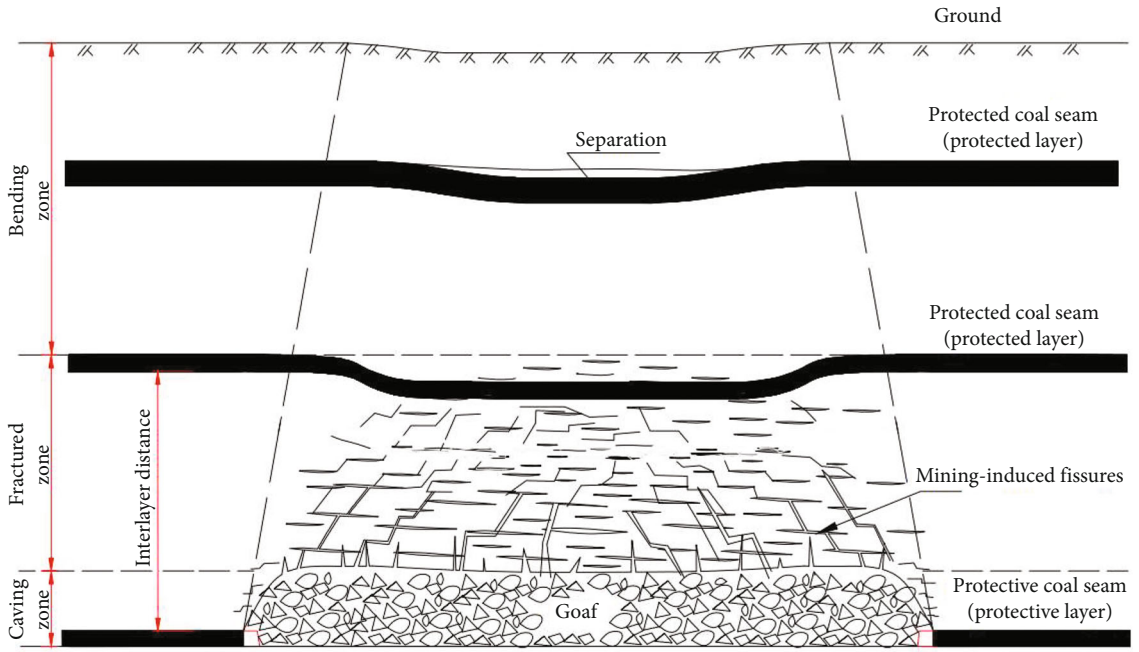

Figure 2: Illustration diagram for lower protective layer mining.

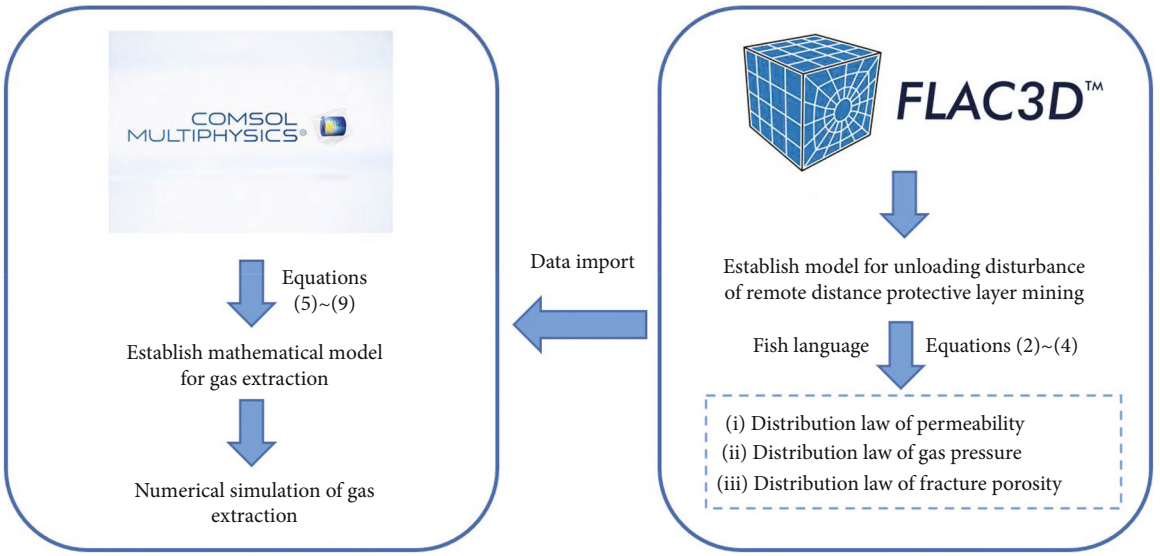

Figure 3: Numerical simulation flowchart.

Table 2: Physicomechanical parameters for each rock layer.

Rock formation	Elasticity moduli (GPa)	Tensile strength (MPa)	Cohesion (MPa)	Friction angle (°)	Poisson's ratio	Density (kg/m^3)
Overlying strata	2.2	2.7	6.6	37	0.20	1900
Siltstone	5.0	5.4	6.2	40	0.25	2500
Sandy mudstone	3.0	3.5	3.7	32	0.23	2530
Claystone	1.8	1.1	3.0	32	0.20	1900
Mudstone	2.0	2.5	2.7	30	0.18	2430
Coal seam	1.0	1.0	2.0	28	0.21	1300
Kaolinite rock	1.8	2.5	4.0	35	0.24	2400
Lower strata	3.0	2.0	4.6	40	0.25	2500

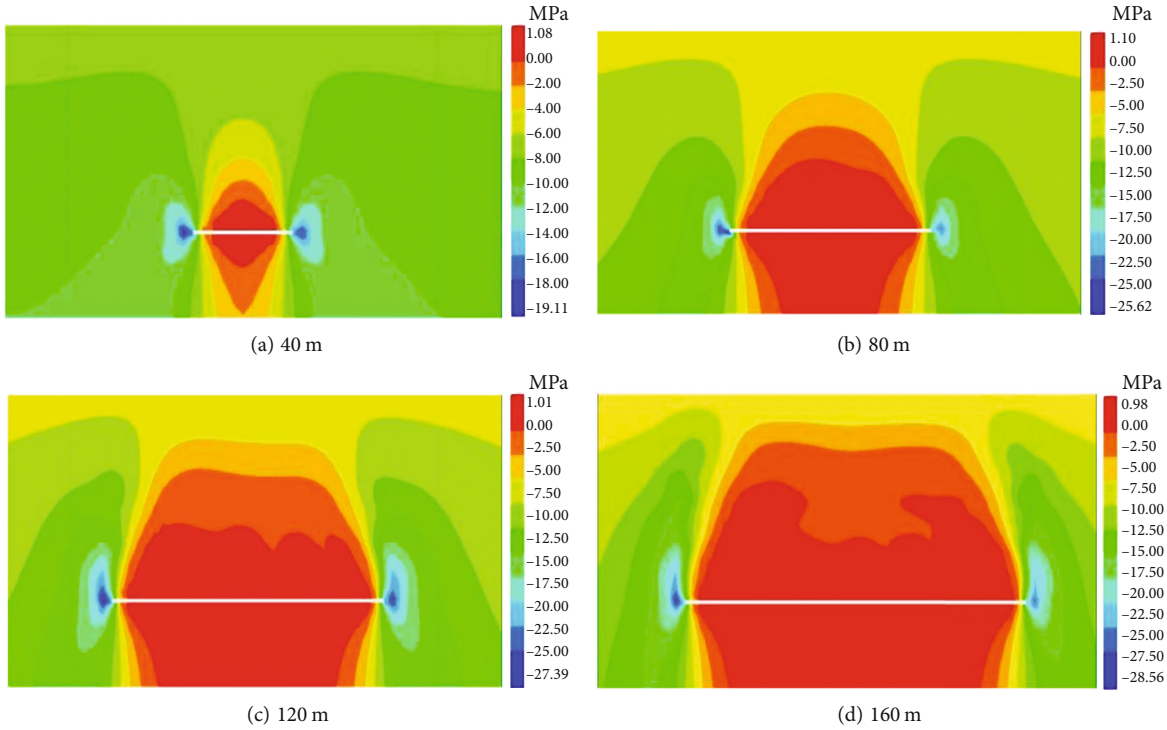

Figure 4: Distributions of vertical stress along strike direction at different advancing distances.

where k_0 and k represent the coal permeability before and after unloading disturbance, mD; Θ_0 and Θ represent volumetric stress of coal seam before and after unloading disturbance, Pa; ξ is the permeability jump coefficient; and b_σ represents the influencing coefficient of volumetric stress, Pa^{-1}.

3.1.2. Evolution Model for Gas Pressure. As previously stated, the geostress state of the protected layer changes during protective layer mining, resulting in the deformation of protected layer. Due to deformation of protected layer, there is an imbalance of gas pressure in the fissures of coal body. In other words, the balance between gas desorption and adsorption is broken, and a small amount of adsorbed gas is transformed into its free state. Taking into characteristics of the remote distance protective layer mining into account, evolution model for gas pressure is built according to assumptions: (A1) coal is a dual-porosity medium saturated with coal gas; (A2) gas content within the protected layer is kept constant prior to gas extraction; and (A3) variation of macroscopic volume of the coal seam at stage one is dominated by fracture expansion, with variation of coal matrix porosity ignored. The fracture porosity is given by assumptions (A1) and (A3):

$$\phi_f = \phi_{f0} + \Delta\varepsilon_v, \tag{3}$$

where ϕ_{f0} denotes original coal fracture porosity before unloading, ϕ_f denotes coal fracture porosity after unloading, and $\Delta\varepsilon_v$ denotes increment of coal volumetric strain.

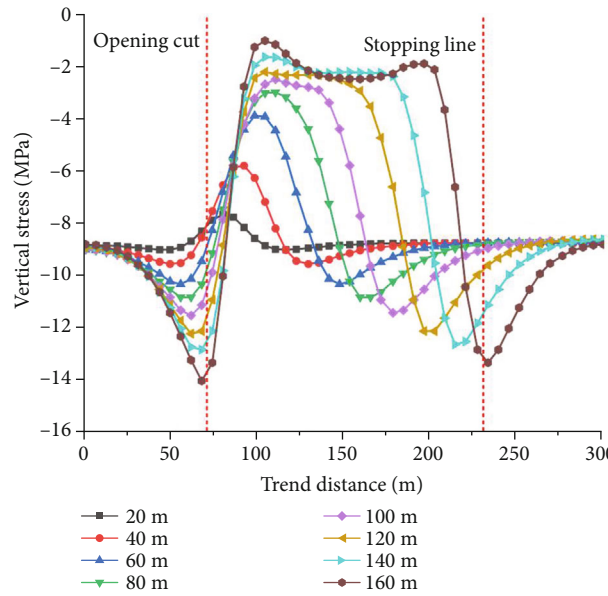

Figure 5: Vertical stress curves for upper C_{19} protected layer at varying advancing distances.

With the expansion of fractures in protected layer, gas adsorbed in coal matrix pores is desorbed and then diffuses to coal fracture due to gas concentration difference, causing fracture gas pressure to vary. As coal gas pressure is affected by both unloading disturbance and gas extraction, fracture gas pressure after the unloading protected layer is reckoned

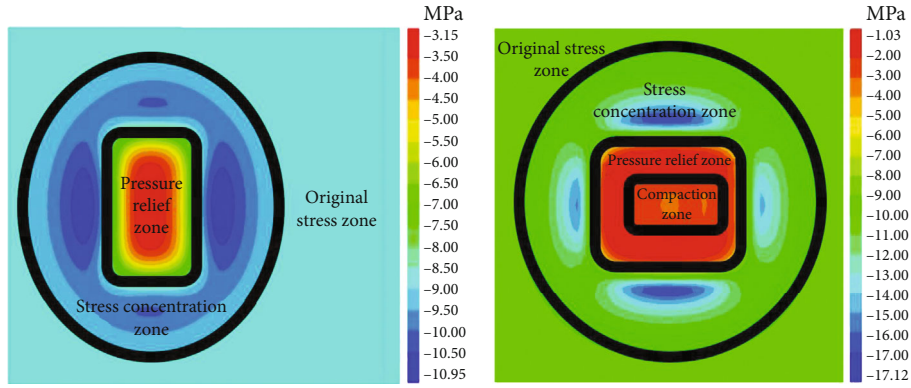

(a) 80 m (b) 160 m

Figure 6: Distributions of vertical stress along bedding plane of protected layer at varying advancing distances.

as a transition variable to connect them. According to assumption (A2), the transition gas pressure can be obtained after an unloading disturbance:

$$\frac{V_L p}{p+P_L}\rho_s\rho_a + \phi_m\frac{M_c}{RT}p + \phi_f\frac{M_c}{RT}p = \left(\frac{V_L p_0}{p_0+P_L}\rho_s\rho_a + \phi_m\frac{M_c}{RT}p_0 + \phi_{f0}\frac{M_c}{RT}p_0\right)\frac{1}{1+\phi_f-\phi_{f0}}, \tag{4}$$

where P_L and V_L denote Langmuir pressure and volume, respectively, ρ_a denotes coal density, ρ_s denotes coal gas density in the standard state, M_c denotes gas molecule mass, T denotes coal body temperature, R denotes ideal gas constant, p denotes transition gas pressure after unloading disturbance, and p_0 denotes original gas pressure.

Since Equation (4) only contains unknown variables of gas pressure p and fracture porosity ϕ_f, it establishes the relationship between gas pressure and fracture porosity after unloading disturbance.

3.2. Mathematical Model for Gas Extraction. The preceding sections have described characteristic changes caused by mining disturbance prior to gas extraction for remote distance protective layer mining. After unloading disturbance, gas extraction is implemented under the unloading state of protected layer. As mentioned before, the transition gas pressure is a parameter that represents an initial condition of gas pressure during gas extraction. Meanwhile, unloading disturbance causes variation of coal permeability and porosity; thus, initial values for coal permeability and porosity during gas extraction are the corresponding coal permeability and porosity after unloading disturbance. In short, the preceding sections provide initial conditions for subsequent gas extraction simulation.

3.2.1. Controlling Equation of Coal Deformation. The controlling equation could be derived in combination with the constitutive relationship, strain-displacement equation, and stress equilibrium equation of coal body. Based on assumption (A1), the principle of effective stress, and strain induced by gas sorption [22], the controlling equation of coal deformation is given as

$$\frac{G}{1-2\nu}u_{j,ji} + Gu_{i,jj} - K\varepsilon_{s,i} - \beta_m p_{m,i} - \beta_f p_{f,i} + f_i = 0, \tag{5}$$

where K and G represent coal bulk and shear moduli, u_i represents displacement in ith direction, ν represents Poisson's ratio of coal, β_f and β_m represent corresponding coefficients for fracture and matrix pore, p_m and p_f represent matrix and fracture gas pressure, ε_s represents strain induced by gas sorption, and f_i represents the ith component of coal body force.

3.2.2. Controlling Equation of Gas Migration. The adsorption-desorption equilibrium of coal seam would be broken during gas drainage. Matrix gas would diffuse into

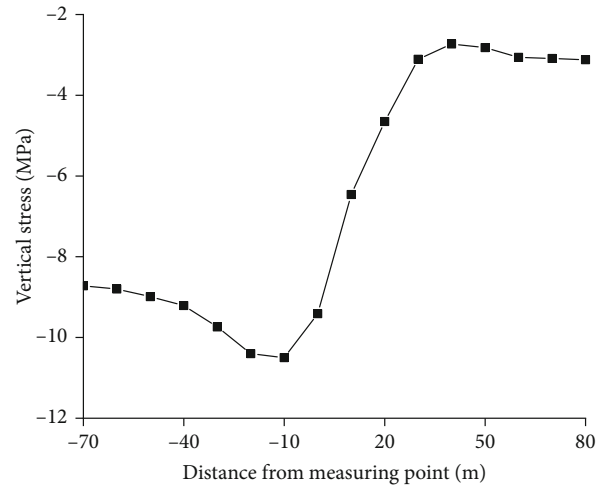

Figure 7: Vertical stress variation of a central measuring point in protected layer.

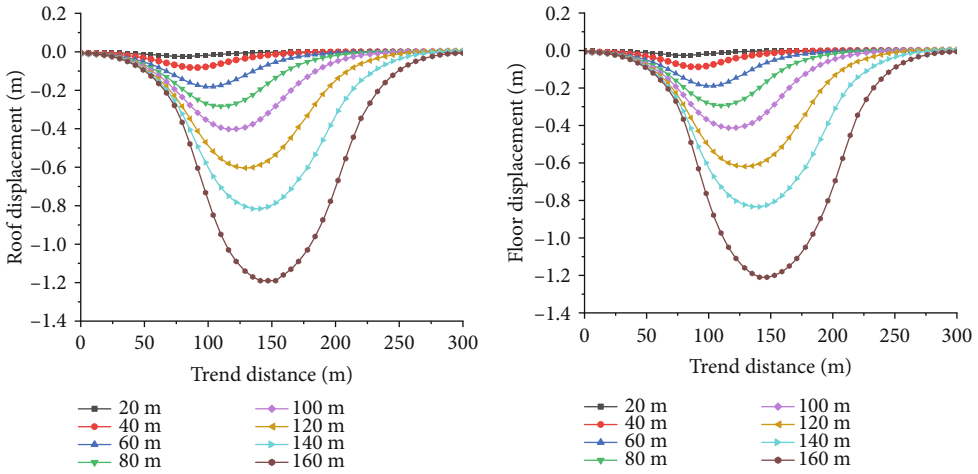

(a) Roof displacement (b) Floor displacement

Figure 8: Displacement curves of C_{19} protected layer at different advancing distances.

coal fracture obeying Fick's law. Governing equation for matrix gas pressure evolution can be derived based on continuity equation [22]:

$$\frac{\partial p_m}{\partial t} = \frac{V_M\left(p_m - p_f\right)\left(p_m + P_L\right)^2}{\tau V_L R T P_L \rho_a + \tau \phi_m V_M \left(p_m + P_L\right)^2}, \tag{6}$$

where τ represents the adsorption time, d, and V_M represents the gas molar volume in standard state, L/mol.

The gas seepage in coal fracture also satisfies continuity equation, and then, the governing equation for fracture gas pressure evolution is obtained [22]:

$$p_f \frac{\partial \phi_f}{\partial t} + \phi_f \frac{\partial p_f}{\partial t} + \frac{1}{\tau}\left(p_f - p_m\right)\left(1 - \phi_f\right) = \nabla \bullet \left(\frac{k}{\mu} p_f \nabla p_f\right), \tag{7}$$

where μ represents gas dynamic viscosity.

Assuming the coal body as a dual-porosity media with single permeability and ignoring variation of matrix porosity [22], the coal fracture porosity with sorption-induced strain considered is given by

$$\frac{\phi_f}{\phi_{f0}} = 1 + \frac{\beta_f}{M}\left(p_f - p_0\right) + \frac{\beta_m}{M}\left(p_m - p_0\right) + \left(\frac{K}{M} - 1\right)\left(\frac{\varepsilon_l p_m}{p_m + P_L} - \frac{\varepsilon_l p_0}{p_0 + P_L}\right), \tag{8}$$

where ε_l denotes the ultimate adsorption expansion deformation of coal body.

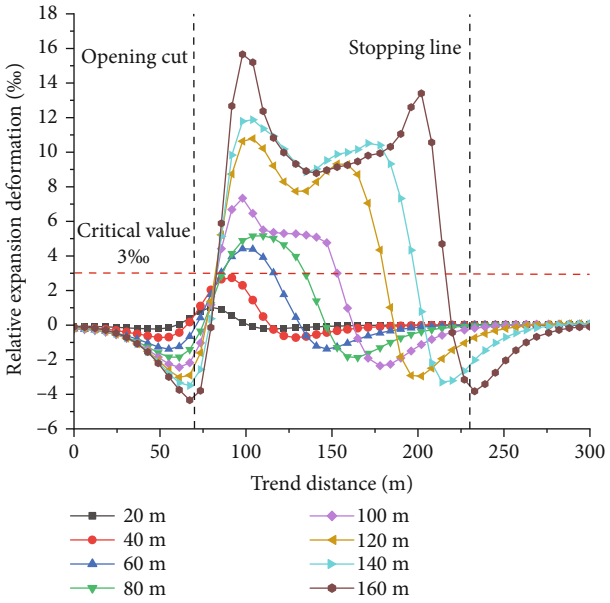

Figure 9: Deformation curves for C_{19} protected layer at different advancing distances.

In accordance with the cubic relation between porosity and coal fracture permeability [22], fracture permeability is expressed as

$$\frac{k}{k_0} = \left\{1 + \frac{\beta_f}{M}\left(p_f - p_0\right) + \frac{\beta_m}{M}\left(p_m - p_0\right) + \left(\frac{K}{M} - 1\right)\left(\frac{\varepsilon_l p_m}{p_m + P_L} - \frac{\varepsilon_l p_0}{p_0 + P_L}\right)\right\}^3. \tag{9}$$

Equations (5)–(9) are coupled governing equations for gas extraction, in which coal deformation, gas diffusion,

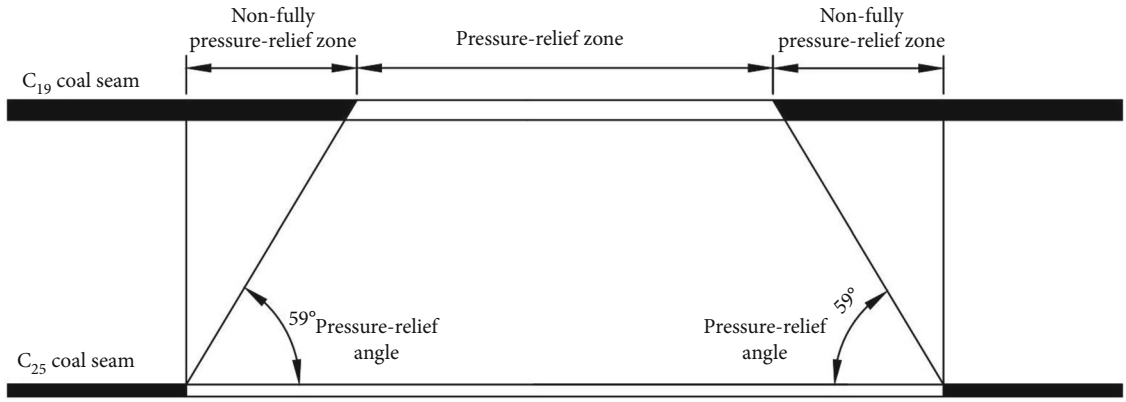

Figure 10: Pressure-relief angle and corresponding zones of protected layer.

gas seepage, and fracture permeability evolution are all considered.

4. Numerical Simulation of Unloading Disturbance and Gas Extraction

4.1. Numerical Simulation Workflow. Currently, COMSOL Multiphysics program has been extensively adopted to analyze multiphysics coupled problems [23]. Nonetheless, when it is adopted in solving large deformation occurred by mining engineering, its convergence becomes relatively poor, especially in three-dimensional problems. The FLAC^{3D} program, a finite difference code with high accuracy for large deformation problems, is adopted instead to solve the deformation field before gas extraction. Hence, in this work, numerical simulation is conducted by combining the COMSOL Multiphysics and FLAC^{3D} programs. The detailed simulation flowchart is illustrated in Figure 3. Firstly, the FLAC^{3D} program is utilized to obtain deformation and stress of C_{19} protected layer due to unloading mining of C_{25} protective layer. Secondly, Fish language (secondary development language embedded in FLAC^{3D}) is used in accordance with Equations (2)–(4) to obtain permeability, fracture porosity, and gas pressure in C_{19} protected coal seam. Thirdly, the geometric model for C_{19} protected layer is reconstructed in COMSOL Multiphysics program, and then, permeability, fracture porosity, and gas pressure data obtained in the FLAC^{3D} program, which are used as an initial condition, are input to COMSOL to study gas migration during gas extraction. The following results indicate that unidirectional sequential coupling of FLAC^{3D} and COMSOL Multiphysics programs can simulate characteristic changes of remote distance protective layer mining accurately.

4.2. Characteristic Changes during Unloading Disturbance of Remote Distance Protective Mining. According to mining conditions of C_{25} protective layer in Chajiaotan mine, a FLAC^{3D} numerical model is built based on the lithology columnar as illustrated in Figure 1. Table 2 gives the corresponding parameters adopted in numerical simulation. During numerical simulation, the C_{25} protective layer is mined with a step length of 10 m, and distributions of stress, displacement, and strain are stored and analyzed after each step.

Table 3: Calculation parameters used in study.

Parameter	Values
Initial matrix porosity, ϕ_{m0}	0.06
Initial permeability, k_0	2.8×10^{-4} mD
Initial fracture porosity, ϕ_{f0}	0.012
Initial gas pressure, p_0	2.06 MPa

4.2.1. Results of Vertical Stress and Analysis. With the excavation of C_{25} protective layer, stresses within surrounding rock would be redistributed. Vertical stress distributions in surrounding rock along the strike direction at different advancing distances (i.e., 40 m, 80 m, 120 m, and 160 m) are depicted in Figure 4. As can be seen, stress concentration zones with vertical stress greater than its original value occur on both sides of the working face, while pressure-relief zones are located at the floor and roof of working face; morphology of vertical stress distribution in the surrounding rock is nearly symmetrical. With the working face of C_{25} protective layer advancing forward, zones of stress concentration and pressure relief increase continuously. The peak vertical stress on both sides of working face increases from 19.1 MPa to 25.6 MPa with the working face of C_{25} protective layer advancing from 40 m to 80 m. However, when the advancing distance is changed from 120 m to 160 m, the variation of vertical peak stress is relatively minor, and vertical stress remains basically stable.

With the advancement of lower C_{25} protective layer, vertical stress curves for the upper C_{19} protected layer at varying advancing distances are obtained and illustrated in Figure 5.

As seen in Figure 5, vertical stress in C_{19} protected layer is less affected by protective layer mining with advancing distance of C_{25} protective layer being less than 20 m. When advancing distance is 40 m, maximum and minimum

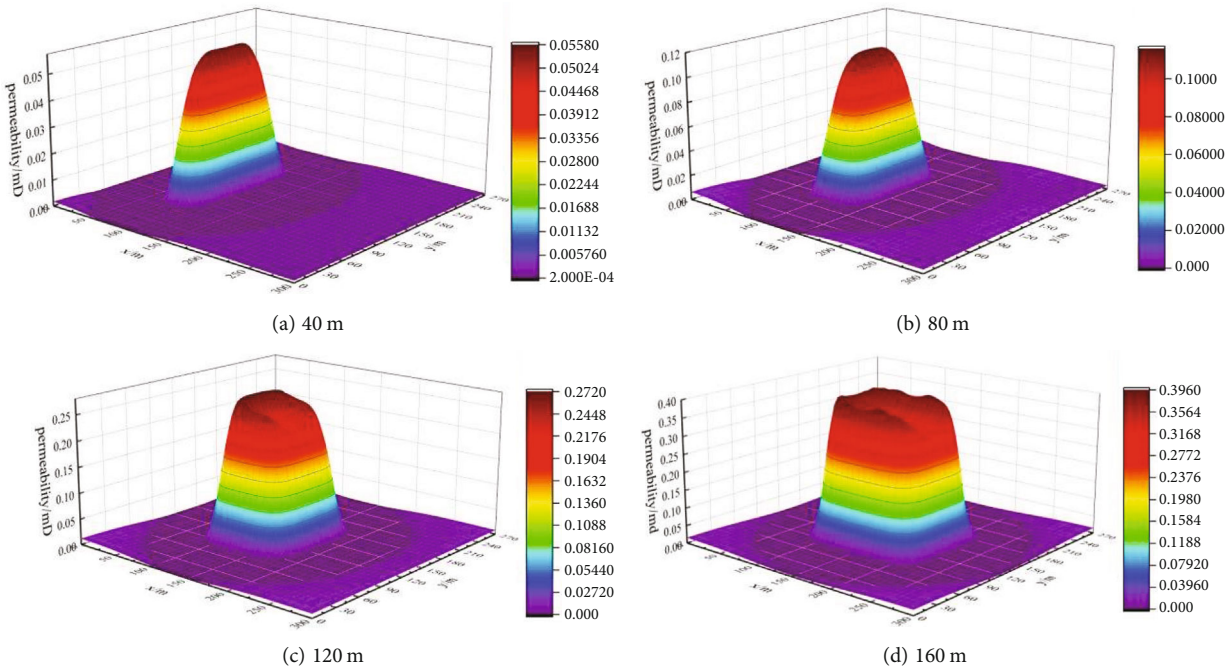

Figure 11: Permeability evolutions of protected layer at different advancing distances.

vertical stresses within the protected layer are -9.0 MPa and -7.6 MPa (negative denotes compression stress), respectively, which indicates that the coefficient of vertical stress concentration reaches 1.03 and maximum pressure-relief stress is 12.9% lower than its original vertical stress. With the continuous increase of advancing distance (e.g., 60 m ~ 80 m), mining influence of C_{25} protective layer on protected layer would gradually increase, which are represented by the increase of stress concentration coefficient, pressure-relief, and stress concentration zones and decrease of vertical stress within the pressure relief zone. When advancing distance is 120 m, the maximum vertical stress is -12.1 MPa (i.e., with concentration coefficient of stress being 1.39), and minimum vertical stress is -2.2 MPa, which is 74.8% lower than its original vertical stress. When the advancing distance reaches to an extent (e.g., 140 m), the vertical stress in the pressure relief zone begins to recover resulting from the roof compaction effect of protected layer, and the vertical stress in this zone presents a saddle-shaped distribution.

Figure 6 presents distributions of vertical stress along the bedding plane of protected layer at varying advancing distances.

As shown in Figure 6, the vertical stress along bedding plane of protected layer varies in different zones. At the advancing distance of 80 m, the zone with increased vertical stress is from 44 m ahead to 3 m in the rear of the open-off cut, the zone with decreased vertical stress is from 3 m to 80 m in the rear of open-off cut, and other zone with vertical stress kept unchanged is from 44 m to 80 m ahead of open-off cut. Therefore, according to distribution characteristics of vertical stress, the protected layer with advancing distance being 80 m could be subdivided into three different zones as illustrated in Figure 6(a). Furthermore, when the advancing

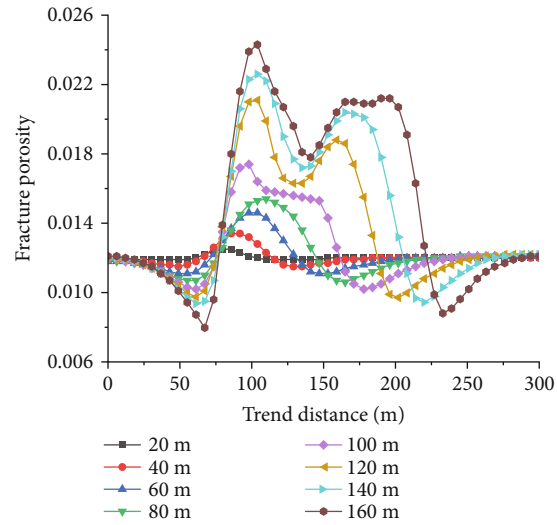

Figure 12: Fracture porosity evolutions of protected layer at varying advancing distances.

distance reaches to an extent (e.g., 140 m), the zone whose vertical stress had been significantly released starts to recover again. Therefore, after the protective layer mining ended (i.e., an advance distance of 140 m), the protected layer could be subdivided into four different zones as illustrated in Figure 6(b).

The vertical stress variation of a measuring point, located at the corresponding center of working face of C_{25} protective layer, was also monitored. Figure 7 gives the vertical stress variation of a central measuring point in protected layer.

As shown in Figure 7, when the measuring point is located ahead of C_{25} working face, vertical stress would be

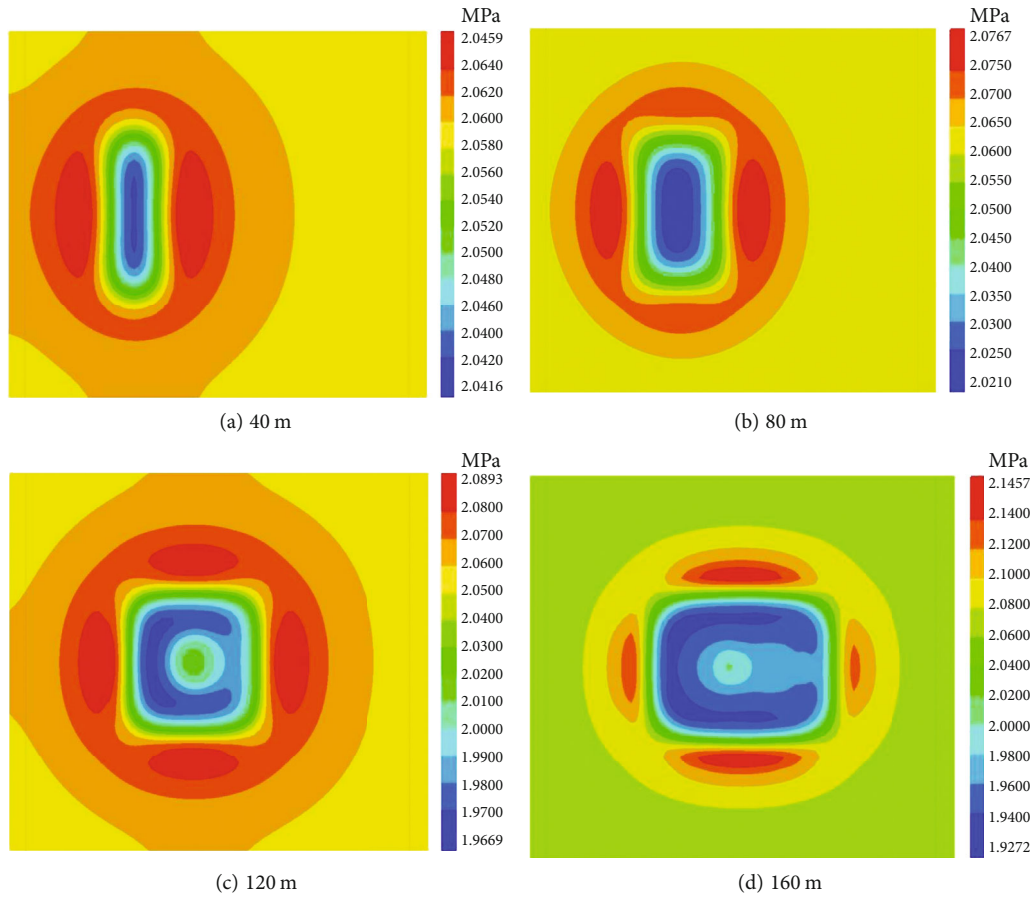

Figure 13: Gas pressure evolutions of protected layer at different advancing distances.

increased. However, when C_{25} working face has passed the measuring point (e.g., 5 m), the vertical stress of measuring point decreases due to the unloading mining affect. If C_{25} working face continues advancing to an extent, vertical stress of measuring point would tend to be stable. The results are consistent with the previous analysis. From the perspective of stress evolutions, the C_{19} protected layer experienced a process of stress loading, stress unloading, stress recovery, and stress stability.

4.2.2. Results and Analysis of Relative Expansion Deformation. Figure 8 presents the roof and floor displacement curves for C_{19} protected layer at different advancing distances, based on which the relative expansion deformation of C_{19} protected layer is calculated:

$$\varsigma = \frac{d_f - d_r}{m} \times 1000, \tag{10}$$

where ς is the relative expansive deformation of protected layer, ‰; d_f and d_r are the roof and floor displacements of protected layer, respectively, m; and m is the thickness of protected layer, m.

Through calculation, the relative expansion deformation curves of protective layer at different advancing distances are shown in Figure 9. If the relative expansion deformation of protected layer has a magnitude greater than 3‰, it could be considered that the coal permeability has increased significantly and the outburst risk of protected layer would be eliminated [20]. Hence, taking the relative expansion

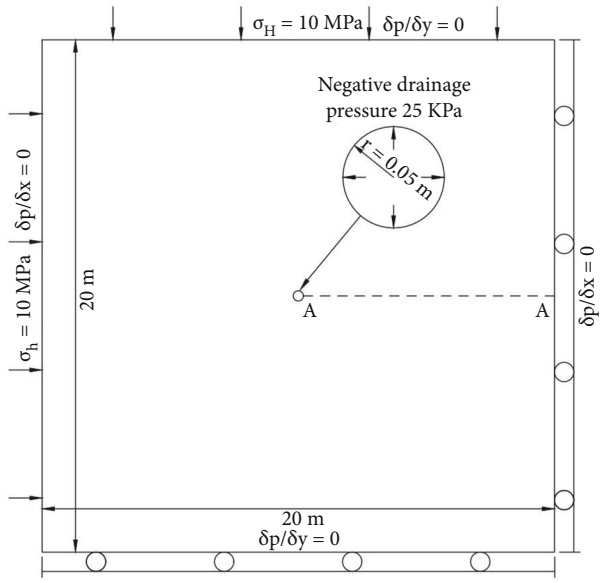

Figure 14: Schematic diagram for gas extraction simulation.

Table 4: Calculation parameters for gas extraction simulation.

Parameters	Values	Parameters	Values
Langmuir constant, P_L	1.41 MPa	Langmuir constant, V_L	0.0228 m^3/kg
Poisson's ratio, ν	0.21	Coal elastic moduli, E	1×10^9 Pa
Elastic moduli for coal matrix, E_m	3×10^9 Pa	Adsorption time, τ	1 d
Methane molar mass, M_c	0.016 kg/mol	Coal density, ρ_a	1300 kg/m^3
Ambient temperature, T	293 K	Ideal gas constant, R	8.314 J/(mol·K)
Langmuir strain constant, ε_L	0.004	Dynamic viscosity of gas, μ	1.081×10^{-5} Pa·s

deformation of 3‰ as the discrimination value, effective pressure-relief angle in strike direction for C_{19} protected layer obtained is 59°.

Based on the pressure-relief angle, the corresponding zone of C_{19} protected layer can be subdivided into the fully pressure-relief zone and nonfully pressure-relief zone as illustrated in Figure 10.

4.2.3. Results and Analysis of Permeability, Fracture Porosity, and Gas Pressure. As mentioned in Section 3.1, the permeability, fracture porosity, and gas pressure would change due to the unloading disturbance of protective layer. The permeability, fracture porosity, and gas pressure are calculated using the Fish language according to Equations (2)–(4). Table 3 lists calculation parameters used in numerical simulation.

Through calculation, evolutions of permeability, fracture porosity, and gas pressure of protected layer during C_{25} protective layer mining are illustrated in Figures 11–13, respectively.

The permeability variation of C_{19} protected layer is on contrary to stress (see Figure 11). In other words, the permeability in the protected layer would be decreased in stress-concentration zone, while it is increased in the pressure-relief zone, which are consistent with the theoretical analysis. With working face continuously advancing, the permeability of protected layer can be increased by 1429 times after the stress decreases significantly. The permeability increase resulting from remote protective layer mining is beneficial for subsequent gas drainage. Moreover, the distributions of gas pressure and vertical stress in protected layer are similar (see Figures 6 and 13). The gas pressure of protected layer is reduced in pressure-relief zone, while it is increased slightly in stress-concentration zone. For an advancing distance of 160 m, the minimum gas pressure in pressure-relief zone is 1.92 MPa, which is 6% lower than the original pressure of 2.06 MPa. The results indicate that although geostress in protected layer is decreased significantly (see Section 4.2.1) due to unloading disturbance, the reduction of gas pressure in protected layer is still relatively minor. Hence, when the remote distance protective layer mining is ended, a measure of gas extraction must be further adopted to decrease gas pressure and thus reducing risks of gas outbursts.

4.3. Characteristic Changes during Gas Extraction Process. To effectively extract coal gas in protected layer, crossing borehole is widely adopted [22]. Gas flow around the crossing borehole of a protected layer is approximate to radial flow. Therefore, a plane strain model is employed to study the gas flow during gas extraction of protected layer after unloading disturbance. The geometric model of C_{19} coal seam is reconstructed in COMSOL Multiphysics program, and permeability, fracture porosity, and gas pressure data obtained in $FLAC^{3D}$ program after unloading disturbance, which are used as initial condition of gas extraction simulation, are input in the form of COMSOL functions [23]. The schematic diagram for gas extraction simulation is illustrated in Figure 14.

The geometric size is 20 m × 20 m (length × width) with the gas extraction borehole diameter being 0.1 m located in model center. To solve the coupled problem, two built-in modules are utilized: one is the "PDE Module" for the gas migration field, and the other is the "Solid Mechanics Module" for coal deformation [23]. The initial and boundary conditions are illustrated in Figure 14. Normal stresses of 10 MPa are applied in inward directions of left and top boundaries, while roller supports are set on bottom and right boundaries. Four outer edges are all set to be zero flux boundaries, and a negative drainage pressure of 25 kPa is set on the borehole wall boundary. Table 4 lists the related calculation parameters for gas extraction simulation.

4.3.1. Results and Analysis of Borehole Gas Extraction before and after Unloading Disturbance. To investigate the unloading disturbance effect on gas extraction, numerical simulation of gas extraction in protected layer with unloading disturbance considered is compared to that with unloading disturbance not considered. The gas pressure distributions with varying gas drainage periods before and after unloading disturbance of protective layer mining are shown in Figures 15 and 16, respectively.

As seen from Figures 15 and 16, cloud distributions of gas pressure can be regarded as concentric circles; the gas pressure on the borehole wall, a negative drainage pressure of 25 kPa, is the smallest; the greater the distance from borehole center, the greater the gas pressure. Gas pressure at a permanent position around the borehole would gradually decrease with gas drainage time, but its decreased amount is not significant. For instance, when the drainage time changes from 30 d to 180 d, the influence range is relatively constant. The reason is that the original coal permeability before unloading disturbance is low, resulting in the low flow velocity of gas (see Figure 15). Compared to the gas extraction before unloading disturbance, the effect of gas

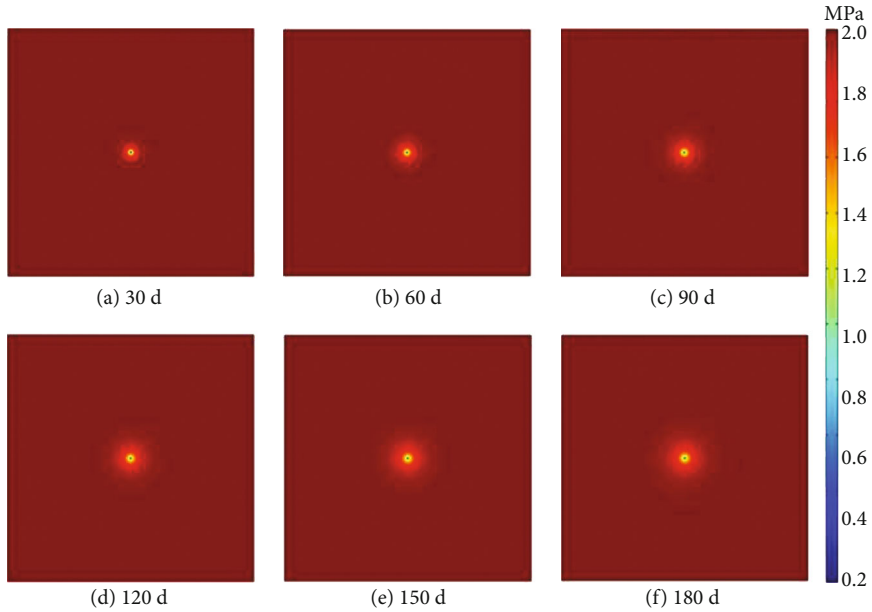

Figure 15: Distributions of gas pressure at varying gas extraction times before unloading disturbance.

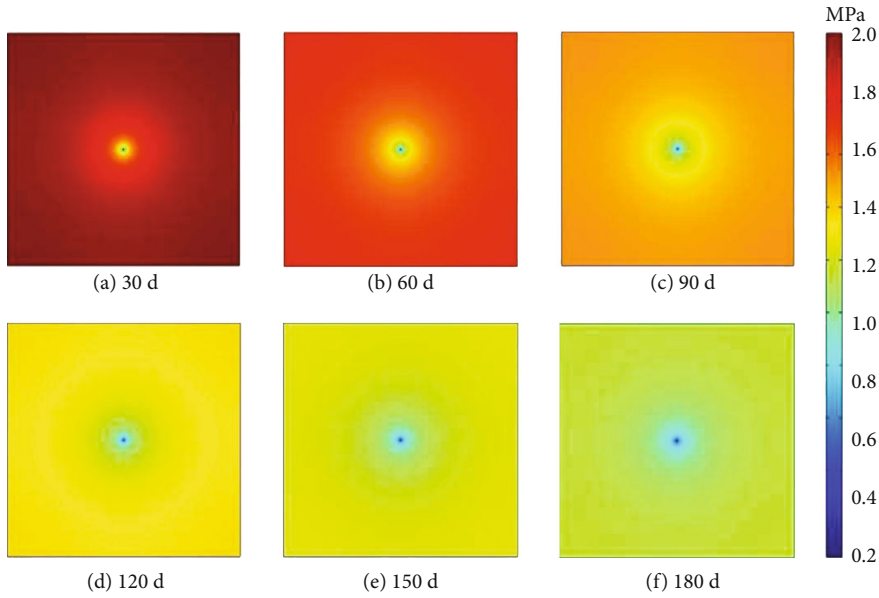

Figure 16: Distributions of gas pressure at varying gas extraction times after unloading disturbance.

extraction on gas pressure after unloading disturbance has changed significantly as illustrated in Figure 16, from which gas pressure within simulation domain has been changed. For instance, gas pressure in the simulation domain could be decreased to an extent even with a short gas extraction time of 30 days, as illustrated in Figure 16(a).

Figure 17 shows variation curves for fracture porosity and gas pressure of a monitoring point with radial distance being 0.5 m from the center of gas extraction borehole.

As described in Figure 17, gas pressure is reduced sharply at the initial phase of gas extraction. However, its decline rate would gradually reduce and gas pressure tends to reach a stable state. In other words, the velocity of gas flow would decrease with gas extraction time increasing. The reason is that, according to the principle of effective stress and Equation (9), the effective coal stress would increase with gas pressure decreasing, resulting in a compression state for coal skeleton and decreases of fracture porosity and permeability. It should be also noted that although the gas desorption will lead to coal matrix shrink (see Equation (5)) followed by expansion of coal fracture and increase of fracture porosity, the final variation of fracture porosity is attributed to the two competition effects between effective stress and gas sorption. As illustrated in Figure 17, the porosity of coal fracture has gradually been decreased, demonstrating that the increase of effective stress caused by gas

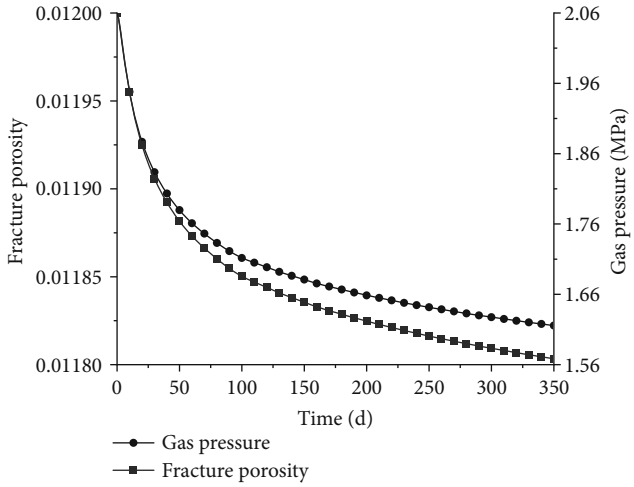

Figure 17: Variation curves for fracture porosity and gas pressure of monitoring point.

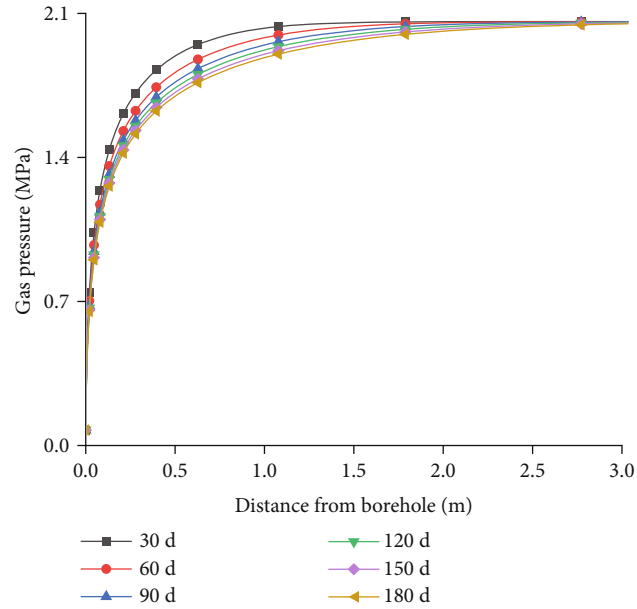

Figure 18: Variation curves for gas pressure before unloading disturbance.

pressure reduction plays a greater role in the compression of fractures than the volume expansion of fractures caused by gas desorption.

To further describe the gas pressure evolution in the protected layer before and after the unloading disturbance, a measuring line (i.e., "*A*-*A*" line in Figure 14) is arranged along radial direction of the borehole. Variation curves for gas pressure on the measuring line before and after unloading disturbance are obtained as shown in Figures 18 and 19, respectively. As seen from Figure 18, the influence radius before unloading disturbance is only 3 m with a gas drainage time of 180 d due to low coal permeability. Therefore, for low permeability coal seam without unloading disturbance, the gas extraction measure is not efficient for gas outburst elimination. Nonetheless, if the unloading disturbance of protective layer mining is considered, gas pressure on the measuring line (see Figure 19) is reduced significantly with gas drainage time increasing, and gas pressure within the whole simulation domain has been influenced; the greatest gas pressure is 1.58 MPa (0.90 MPa) with gas drainage time of 30 d (180 d). In comparison with the two numerical results, it demonstrates that gas extraction combined with remote protective layer mining can reduce gas pressure effectively, which is beneficial for eliminating the outburst risk of protected layer.

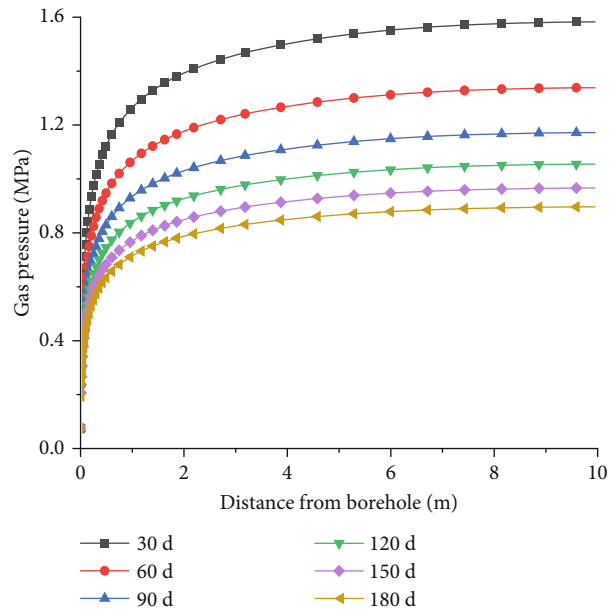

Figure 19: Variation curves for gas pressure after unloading disturbance.

4.3.2. Reasonable Borehole Spacing in Different Pressure Relief Zones

(1) Reasonable Borehole Spacing in a Fully Pressure-Relief Zone. To determine reasonable borehole spacing in the fully pressure-relief zone (see Figure 10), according to the literature [24], five cases of gas extraction with borehole spacing being 20 m, 25 m, 30 m, 35 m, and 40 m are simulated, respectively. The gas pressure-time curves for monitoring point under varying borehole spacings are given in Figure 20. On basis of the "provisions" of China [20], if the magnitude of residual gas pressure was smaller than 0.74 MPa, it could be regarded that risk of outburst is already eliminated. Thus, we adopt the magnitude of 0.74 MPa as the discrimination criterion to determine reasonable borehole spacing. As seen from Figure 20, when borehole spacing of gas extraction is increased to 35 m, residual gas pressure with gas extraction time of 360 d will become greater than discrimination criterion value, which indicates that the reasonable borehole spacing in the fully pressure-relief zone is 30 m with gas extraction time being 360 d. In other words,

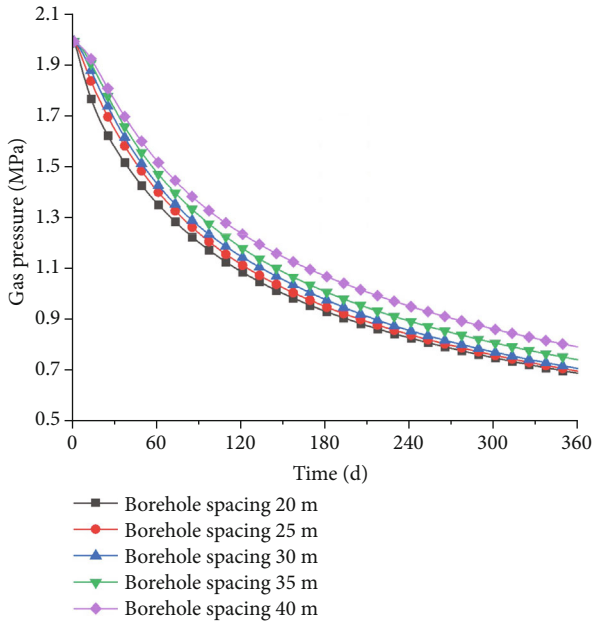

Figure 20: Gas pressure evolutions of monitoring point in fully pressure-relief zone.

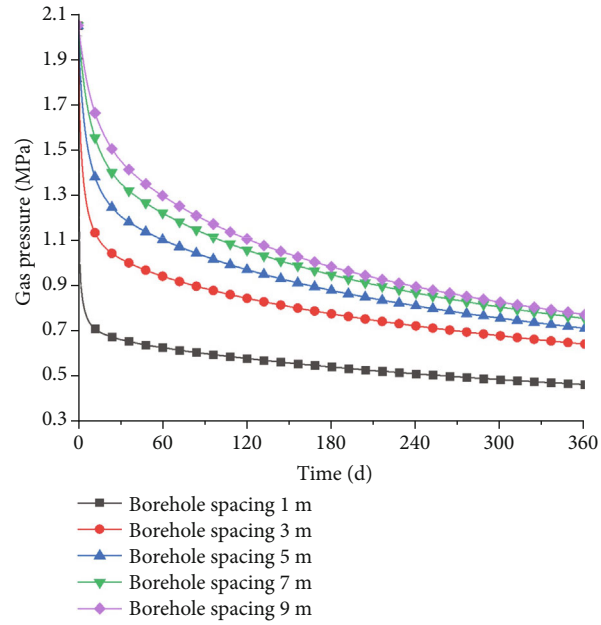

Figure 21: Gas pressure evolutions of monitoring point in nonfully pressure-relief area.

the effective gas extraction radius in fully pressure-relief zone of protected layer in Chajiaotan coal mine is about 15 m.

(2) Reasonable Borehole Spacing in the Nonfully Pressure-Relief Zone. Similarly, five cases of gas extraction with borehole spacing being 1 m, 3 m, 5 m, 7 m, and 9 m are simulated to determine the reasonable borehole spacing in the nonfully pressure-relief zone (see Figure 10). Numerical results of gas pressure-time curves for monitoring point under varying borehole spacings are illustrated in Figure 21. When borehole spacing is increased to 7 m, residual gas pressure at gas extraction time of 360 d will become greater than the discrimination criterion value, implying that the effective gas extraction radius for the fully pressure-relief zone is 2.5 m with gas extraction time being 360 d. Therefore, the reasonable borehole spacing of gas extraction for Chajiaotan coal mine in the nonfully pressure-relief zone is about 5 m.

5. Field Application and Validation

5.1. Borehole Layout for Gas Extraction. To intercept and extract the pressure-relief gas of C_{19} protected layer after unloading disturbance of protective layer mining, crossing boreholes are arranged in the roadway of C_{25} protective layer. On one hand, such layout of crossing boreholes can effectively save the construction cost of roadway or boreholes and shorten the preparation period. On the other hand, crossing boreholes would effectively cover the corresponding C_{19} protected layer, which ensures that all free gas would be efficiently intercepted and drained by the gas extraction boreholes, thus decreasing gas pressure or content of C_{19} protected layer to reduce its outburst risk.

As mentioned in Section 4.2.2, the corresponding C_{19} protected layer can be subdivided into the fully pressure-relief zone and nonfully pressure-relief zone. Moreover, numerical simulations of gas drainage after unloading disturbance indicated that the effective gas drainage radii are 15 m and 2.5 m in the fully pressure-relief zone and nonfully pressure-relief zone, respectively. Therefore, according to the engineering mining plan of Chajiaotan coal mine, borehole spacings of gas extraction in the fully and nonfully pressure-relief zones are set to be 30 m and 5 m, respectively.

5.2. Investigation on Residual Gas Pressure. According to "provisions" of China [20], if residual gas pressure was below 0.74 MPa, then it could be regarded that the outburst risk was already eliminated. Hence, the outburst elimination effect of C_{19} protected layer is further investigated by analyzing residual gas pressure in C_{19} protected layer after gas extraction. Eleven gas pressure inspection boreholes are designed, among which five inspection boreholes (i.e., boreholes $P_{z1} \sim P_{z5}$) and six inspection boreholes (i.e., boreholes $P_{q1} \sim P_{q5}$) are located along the strike and dip direction of coal seam, respectively, as illustrated in Figure 22.

After C_{25} protective layer mining was ended, the residual gas pressures in inspection boreholes were gathered. Table 5 lists the observed residual gas pressures in these inspection boreholes.

As seen from Table 5, residual gas pressure values in eleven investigated boreholes are all less than discrimination value, which indicate that outburst risk in C_{19} protected layer is effectively decreased by remote protective layer mining in combination with gas extraction, which also verifies the rationality of borehole layout proposed for gas extraction in remote protected layer and reliability of mathematical model and its implementation.

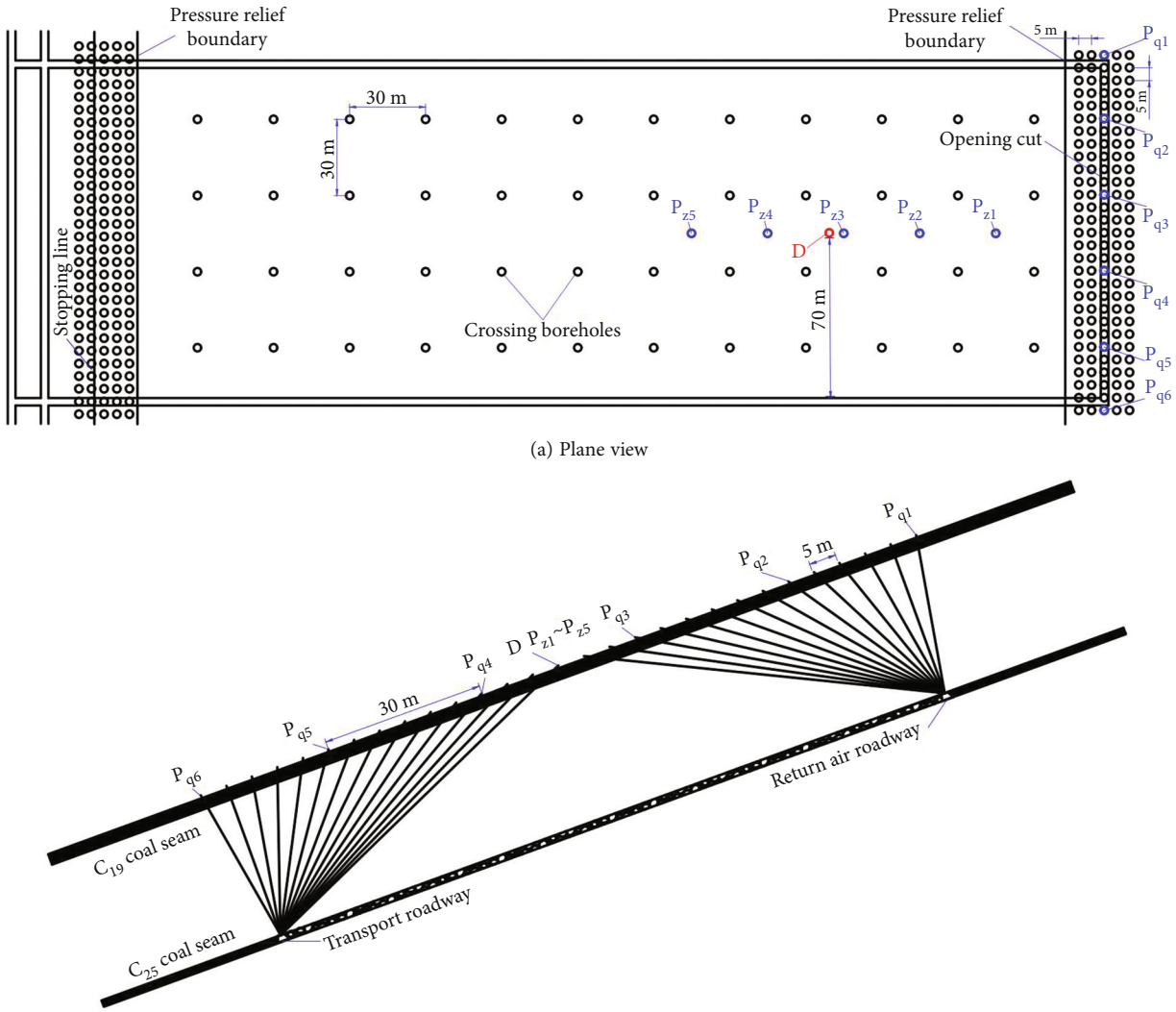

Figure 22: Layout of crossing boreholes.

Table 5: Residual gas pressure in inspection boreholes.

Borehole	Residual gas pressure (MPa)	Borehole	Residual gas pressure (MPa)
P_{q1}	0.45	P_{z1}	0.31
P_{q2}	0.39	P_{z2}	0.29
P_{q3}	0.34	P_{z3}	0.22
P_{q4}	0.29	P_{z4}	0.26
P_{q5}	0.30	P_{z5}	0.20
P_{q6}	0.36		

5.3. Investigation on Relative Expansion Deformation in Protected Layer. To further investigate and validate the unloading disturbance of remote protective layer mining, an inspection point (the *D* point as shown in Figure 22(a)) in C_{19} protected layer was designed to investigate the relative expansion deformation with working face of protective layer advancing. The inspection point is situated along dip direction of C_{25} protected layer, 70 m away from the opening cut of protective layer. The variation curve for relative expansion deformation for C_{19} protected layer during C_{25} protective layer mining is given in Figure 23.

As shown in Figure 23, when the inspection point is located ahead of working face, the relative expansion deformation is negative, and its minimum value is -3.8‰, which means that the inspection point is in the compression state affected by stress concentration. When the working face of C_{25} protective layer has passed the inspection point, the relative expansion deformation at the inspection point turns from a negative value to a positive value. The relative expansion deformation has reached a maximum value of 14.2‰ when it passes 50 m away from the inspection point. With the working face continuously advancing, relative expansion deformation of the protected layer would tend to be stable. From the perspective of stress evolution, it can be inferred that the C_{19} protected layer experienced processes of stress loading, stress unloading, stress recovery, and stress stability. The field result of the relative expansion deformation of

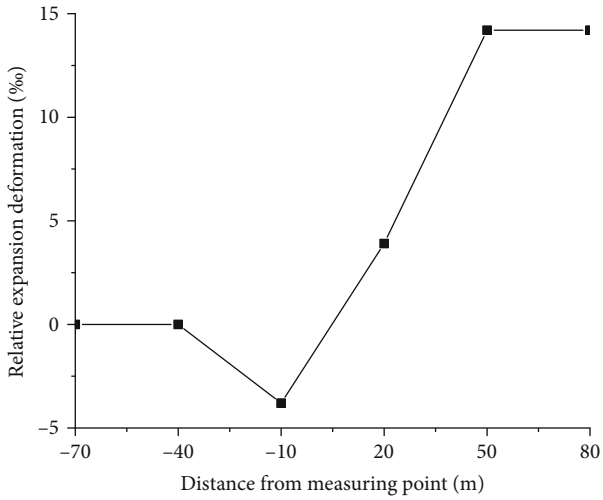

Figure 23: The variation curve for the relative expansion deformation.

inspection point agrees well with numerical simulation (see Section 4.2.2). According to "provisions" of China, if relative expansion deformation for coal seam is more than a magnitude of 3‰, it is deemed that protected coal seam is effectively protected. Thus, it can be inferred that C_{19} protected coal seam has achieved a reasonable unloading effect after remote distance protective layer mining.

In brief, the results demonstrated that the outburst risk of C_{19} protected layer could be reduced due to the unloading disturbance of C_{25} coal seam mining in combination with gas extraction of C_{19} protected layer, which also validates the reliability of the mathematical model and corresponding implementation proposed.

6. Conclusions

A new mathematical model considering unloading disturbance and solid-gas coupling effect during gas extraction was developed for remote distance protective layer mining. The proposed model was implemented by combining the FLAC^{3D} and COMSOL programs to study characteristic changes during remote distance protective layer mining of Chajiaotan mine. The obtained conclusions are as follows:

(1) Numerical results of unloading disturbance indicated that the protected layer would gradually experience stress loading, unloading, stress recovery, and stability as the protective layer's working face advances; the protected layer could be subdivided into concentration zone, pressure-relief zone, compaction zone, and original zone; the effective pressure-relief angle in strike direction of C_{19} protected layer is 59°, and the C_{19} protected layer can be subdivided into the fully pressure-relief zone and nonfully pressure-relief zone

(2) When the stress in protected layer is reduced by 74.8%, the gas pressure in protected layer is only reduced by 6%, but the permeability of protected layer could be increased by 1429 times. Numerical results of unloading disturbance demonstrated that unloading disturbance plays a greater role on coal permeability than gas pressure, so gas drainage measure must be further adopted to reduce gas pressure

(3) Numerical comparisons of gas pressure distributions in the unloading and original protected layer showed that gas extraction of protected layer after unloading disturbance can reduce gas pressure more effectively. Numerical results of gas extraction under varying borehole spacings showed that appropriate borehole spacings are 30 m and 5 m in the fully and nonfully pressure-relief zones

(4) Numerical results are applied in the design of borehole layout for gas extraction, and residual gas pressure in investigated boreholes is all smaller than the discrimination value of 0.74 MPa; the outburst risk of protected layer has been reduced. The numerical simulation results of relative expansion deformation and gas extraction radii agree well with the results of site observation, which demonstrated the reliability of the mathematical model and its realization. The approach is promising for assessing unloading disturbance and gas drainage in the engineering practice of remote protective layer mining

Data Availability

All data used to support findings of present study are included in the submitted article.

Conflicts of Interest

All authors declare that there are no conflicts of interest concerning the publication of this article.

Acknowledgments

This work is financially supported by the National Natural Science Foundation of China (Grant Nos. 51604111 and 51974121) and the Scientific Research Foundation of Hunan Provincial Education Department (Grant No. 16C0654).

References

[1] H. P. Xie, L. X. Wu, and D. Z. Zheng, "Prediction on the energy consumption and coal demand of China in 2025," *Journal of China Coal Society*, vol. 44, no. 7, pp. 949–1960, 2019.

[2] I. Palmer and J. Mansoori, "How permeability depends on stress and pore pressure in coalbeds: a new model," *SPE Reservoir Evaluation & Engineering*, vol. 1, no. 6, pp. 539–544, 1998.

[3] J. S. Liu, Z. W. Chen, D. Elsworth, X. Miao, and X. Mao, "Evaluation of stress-controlled coal swelling processes," *International Journal of Coal Geology*, vol. 83, no. 4, pp. 446–455, 2010.

[4] Y. P. Cheng and Z. J. Pan, "Reservoir properties of Chinese tectonic coal: a review," *Fuel*, vol. 260, article 116350, 2020.

[5] Z. G. Yuan and Y. H. Shao, "Numerical modeling on hydraulic fracturing in coal-rock mass for enhancing gas drainage,"

Advances in Civil Engineering, vol. 2018, Article ID 1485672, 16 pages, 2018.

[6] B. You, J. X. Xu, S. L. Shi, H. Liu, Y. Lu, and H. Li, "Effect of stress and water pressure on permeability of fractured sandstone based on response surface method," *Frontiers in Earth Science*, vol. 8, no. 11, pp. 1–8, 2020.

[7] C. Hao, Y. Cheng, H. Liu, L. Wang, and Q. Liu, "A novel technology for high-efficiency borehole-enlarging to enhance gas drainage in coal seam by mechanical cutting assisted by water jet," *Energy Sources Part A: Recovery Utilization and Environmental Effects*, vol. 41, no. 1, pp. 1336–1353, 2022.

[8] Z. Yuan, Y. Shao, and Z. Zhu, "Similar material simulation study on protection effect of steeply inclined upper protective layer mining with varying interlayer distances," *Advances in civil engineering*, vol. 2019, Article ID 9849635, 14 pages, 2019.

[9] Y. P. Cheng, Q. X. Yu, and L. Yuan, "Experimental research of safe and high-efficient exploitation of coal and pressure relief gas in long distance," *Journal of China University of Mining & Technology*, vol. 33, no. 2, pp. 8–12, 2004.

[10] M. B. Zhang, M. Q. Lin, H. Q. Zhu, D. Zhou, and L. Wang, "An experimental study of the damage characteristics of gas-containing coal under the conditions of different loading and unloading rates," *Journal of Loss Prevention in the Process Industries*, vol. 55, pp. 338–346, 2018.

[11] L. J. Wang and H. W. Zhou, "Stress field evolution law and disturbance characteristic of coal at depth under mining," *Chinese Journal of Rock Mechanics and Engineering*, vol. 38, no. 1, pp. 2944–2954, 2019.

[12] Y. B. Cai, K. Wang, L. Yuan, C. Xu, Q. Fu, and D. L. Kong, "Numerical simulation and verification of unloading damage evolution characteristics of coal and rock mass during deep mining," *Journal of China Coal Society*, vol. 44, no. 5, pp. 1527–1535, 2019.

[13] Y. H. Pang, G. F. Wang, and B. B. Li, "Stress path effect and instability process analysis of overlying strata in deep stopes," *Chinese Journal of Rock Mechanics and Engineering*, vol. 39, no. 4, pp. 682–694, 2020.

[14] D. J. Xue, H. W. Zhou, X. L. Tang, and Y. F. Zhao, "Evolution of mining induced enhancement and distribution of gas permeability in coal seam and surrounding rock," *Journal of China Coal Society*, vol. 38, no. 6, pp. 930–935, 2013.

[15] H. P. Xie, H. W. Zhou, G. M. Cheng, and F. B. Zhou, "On theoretical and modeling approach to mining enhanced permeability for simultaneous exploitation of coal and gas," *Journal of China Coal Society*, vol. 38, no. 7, pp. 1101–1108, 2013.

[16] T. H. Yang, T. Xu, H. Y. Liu, C. A. Tang, B. M. Shi, and Q. X. Yu, "Stress-damage-flow coupling model and its application to pressure relief coal bed methane in deep coal seam," *International Journal of Coal Geology*, vol. 86, no. 4, pp. 357–366, 2011.

[17] X. M. Zhang, D. M. Zhang, C. J. Leo, G. Z. Yin, D. Feng, and D. S. Liyanapathirana, "Damage evolution and post-peak gas permeability of raw coal under loading and unloading conditions," *Transport in Porous Media*, vol. 117, no. 3, pp. 465–480, 2017.

[18] Z. D. Liu, Y. P. Cheng, Q. Q. Liu, J. Jiang, W. Li, and K. Zhang, "Numerical assessment of CMM drainage in the remote unloaded coal body: insights of geostress-relief gas migration and coal permeability," *Journal of Natural Gas Science and Engineering*, vol. 45, pp. 487–501, 2017.

[19] H. Y. Liu, Y. P. Cheng, C. C. Zhao, H. X. Zhou, and Z. P. Zhang, "Classification and judgment method of the protective layers," *Journal of Mining & Safety Engineering*, vol. 27, no. 4, pp. 468–474, 2010.

[20] National Coal Mine Safety Supervision Bureau, *Provisions of the Prevention of Coal and Gas Outburst*, China Coal Industry Publishing House, Beijing, China, 2019.

[21] Z. G. Yuan, J. T. Zhao, S. Q. Li, Z. Jiang, and F. Huang, "A unified solution for surrounding rock of roadway considering seepage, dilatancy, strain-softening and intermediate principal stress," *Sustainability*, vol. 14, no. 13, p. 8099, 2022.

[22] Y. P. Cheng, Q. Q. Liu, and T. X. Ren, *Coal Mechanics*, China Science Press, Beijing, China, 2017.

[23] H. H. Zhang, J. X. Wang, C. J. Fan, H. J. Bi, L. Chen, and C. Y. Xu, "An improved coupled modeling method for coalbed methane extraction after hydraulic fracturing," *Geofluids*, vol. 2022, 15 pages, 2022.

[24] M. Ji, Z. G. Sun, and W. Sun, "A case study on the gas drainage optimization based on the effective borehole spacing in Sima coal mine," *Geofluids*, vol. 2021, no. 2, Article ID 5510566, p. 9, 2021.